

JGR Atmospheres

RESEARCH ARTICLE

10.1029/2022JD037768

Key Points:

- The relationship between the vertical eddy diffusivity and wind speed is different over different underlying surface types
- The vertical eddy diffusivity estimated using the flux and strain rate is comparable to that using the friction velocity and height
- The scaling coefficient for estimating the vertical eddy diffusivity using turbulent kinetic energy varies with surface roughness length

Supporting Information:

Supporting Information may be found in the online version of this article.

Correspondence to:

J. A. Zhang and M. Momen,
jun.zhang@noaa.gov;
mmomen@uh.edu

Citation:

Ming, J., Zhang, J. A., Li, X., Pu, Z., & Momen, M. (2023). Observational estimates of turbulence parameters in the atmospheric surface layer of landfalling tropical cyclones. *Journal of Geophysical Research: Atmospheres*, 128, e2022JD037768. <https://doi.org/10.1029/2022JD037768>

Received 30 AUG 2022

Accepted 7 AUG 2023

Author Contributions:

Conceptualization: Jun A. Zhang, Mostafa Momen

Data curation: Xin Li

Formal analysis: Jie Ming, Xin Li

Funding acquisition: Jun A. Zhang, Zhaoxia Pu





Investigation: Mostafa Momen

Methodology: Jie Ming, Jun A. Zhang, Zhaoxia Pu

Writing – original draft: Jie Ming, Jun A. Zhang, Zhaoxia Pu

Writing – review & editing: Jie Ming, Jun A. Zhang, Xin Li, Zhaoxia Pu, Mostafa Momen

Observational Estimates of Turbulence Parameters in the Atmospheric Surface Layer of Landfalling Tropical Cyclones

Jie Ming^{1,2,3,4} , Jun A. Zhang^{5,6} , Xin Li⁷, Zhaoxia Pu⁷ , and Mostafa Momen⁸ 

¹Key Laboratory for Mesoscale Severe Weather/MOE and School of Atmospheric Science, Nanjing University, Nanjing, China, ²Joint Center for Atmospheric Radar Research of Centre of Modern Analysis, Nanjing University (CMA/NJU), Beijing, China, ³China Meteorological Administration Xiong'an Atmospheric Boundary Layer Key Laboratory, Xiong'an New Area, China, ⁴Lianyungang Institute of High-Tech Research, Nanjing University, Lianyungang, China, ⁵Hurricane Research Division, Atlantic Oceanographic and Meteorological Laboratory, National Oceanographic and Atmospheric Administration, Miami, FL, USA, ⁶Cooperative Institute for Marine and Atmospheric Studies, University of Miami, Miami, FL, USA, ⁷Department of Atmospheric Sciences, University of Utah, Salt Lake City, UT, USA, ⁸Department of Civil and Environmental Engineering, University of Houston, Houston, TX, USA

Abstract This study analyzes observations collected by multilevel towers to estimate turbulence parameters in the atmospheric surface layer of two landfalling tropical cyclones (TCs). The momentum flux, turbulent kinetic energy (TKE) and dissipation rate increase with the wind speed independent of surface types. However, the momentum flux and TKE are much larger over land than over the coastal ocean at a given wind speed range. The vertical eddy diffusivity is directly estimated using the momentum flux and strain rate, which more quickly increases with the wind speed over a rougher surface. Comparisons of the eddy diffusivity estimated using the direct flux method and that using the friction velocity and height show good agreement. On the other hand, the traditional TKE method overestimates the eddy diffusivity compared to the direct flux method. The scaling coefficients in the TKE method are derived for the two different surface types to better match with the vertical eddy diffusivity based on the direct flux method. Some guidance to improve vertical diffusion parameterizations for TC landfall forecasts in weather simulations are also provided.

Plain Language Summary Improved understanding of small-scale processes near the surface is important for advancement of tropical cyclone intensity prediction. Observational data collected by multilevel towers are analyzed to study the turbulent mixing process and structure in the atmospheric surface layer of two landfalling storms. Turbulence parameters such momentum flux, turbulent kinetic energy (TKE) and dissipation rate are estimated, which shows a wind speed independence regardless of surface types. The magnitudes of the momentum flux and TKE are much larger over land than over the ocean at a given wind speed range. The turbulent mixing strength measured by the vertical eddy diffusivity are estimated and compared using three different methods. The scaling coefficient in the eddy diffusivity parameterization is derived based on observations. This newly derived coefficient would potentially lead to improved tropical cyclone forecasts when used in numerical models.

1. Introduction

Turbulent processes in tropical cyclones (TCs) theoretically depend on their intensity (e.g., Emanuel, 1995, 1997, 2012; Montgomery & Smith, 2014). Horizontal diffusion largely regulates the maximum intensity, intensification rate, and structure of a storm (Bryan, 2012; Bryan & Rotunno, 2009; Romdhani et al., 2022; Zhang & Marks, 2015; Zhang et al., 2018). Vertical diffusion, especially in the hurricane boundary layer (HBL), is also a key process for TC intensity and structure variations (e.g., Foster, 2009; Gopalakrishnan et al., 2013; Li et al., 2023; Ma et al., 2018; Rotunno & Bryan, 2012; Zhang et al., 2020). Different types of planetary boundary layer (PBL) schemes with various methods for vertical diffusion parameterizations also produce storms with different intensities and structures in numerical simulations (e.g., Braun & Tao, 2000; Chen et al., 2021; Kepert, 2012; Nolan et al., 2009; Smith & Thomsen, 2010; Zhu et al., 2014).

Analyses of retrospective forecasts of TCs by the operational Hurricane Weather and Research Forecasting (HWRF) model established that the setup of the vertical diffusion in the PBL scheme significantly influences storm size, inflow angle, kinematic PBL heights, and distribution of deep convection close to the eyewall region (Zhang et al., 2015). Other HWRF simulations suggested that vertical diffusion also affects convective activities

and storm size in the outer core region (Bu et al., 2017). These structural differences resulted in different intensity forecasts. For instance, the skill of HWRf forecasts of rapidly intensifying storms varied with the magnitude of the vertical eddy viscosity in the PBL scheme (J. A. Zhang et al., 2017). Decreasing vertical eddy viscosity following observational guidance resulted in faster intensification of a TC and improved the intensity forecasts in HWRf. When the eddy viscosity is smaller in HWRf, the simulated TC has a smaller size, stronger inflow, larger supergradient wind, larger PBL convergence, and stronger and more symmetric deep convection, which is consistent with observed characteristics (Bu et al., 2017; Wang et al., 2018; Zhang & Rogers, 2019). The vertical diffusion parameterization also affected the structural evolution of landfalling TCs in HWRf simulations (Zhang & Pu, 2017; F. Zhang et al., 2017). Specifically, based on sensitivity numerical simulations, F. Zhang et al. (2017) found that strong vertical mixing over land (compared to over the ocean) has a positive impact on numerical simulations of hurricanes over land, with improved track, intensity, synoptic flow, and precipitation simulations.

Despite the important role of turbulent diffusion in TC simulations and forecasts, direct observations of turbulent properties are mainly limited to the PBL of the outer core region and near the top of the inflow layer of the eyewall region (Zhang, Marks, et al., 2011; Zhang et al., 2009). Observational estimates of both vertical and horizontal diffusion in the eyewall region have been reported only by a handful of studies. Analyses of 1 Hz flight-level wind data collected by a research aircraft at ~500 m altitude in two intense hurricanes showed that the vertical eddy viscosity increases with the wind speed (Zhang, Marks, et al., 2011). Observational estimation of the vertical eddy viscosity near the top of the inflow layer of several typhoons confirmed the increasing trend of the eddy viscosity with wind speed (Zhao et al., 2020). Based on high-frequency (40 Hz) aircraft observations at different vertical levels in the PBL of the TC outer core region ($R = 100\text{--}150$ km), Zhang and Drennan (2012) estimated the vertical eddy diffusivities for momentum, heat and moisture. They found that the eddy diffusivities increased with height up to the top of the thermodynamic mixed layer before decreasing with height to the top of the inflow layer. Note that recent unmanned aerial vehicle observations collected momentum flux data in the TC boundary layer (TCBL) that may provide additional information for turbulent diffusion in the future (Cione et al., 2020).

The turbulent structure is often different between surface layer and the outer PBL above the surface layer. Multi-level towers with fast-response wind sensors provided observations of the vertical eddy viscosity and mixing length below 85 m altitude during landfalls of three typhoons (Tang et al., 2018), showing that the vertical eddy viscosity weakly increased with the wind speed at all measurement levels. Of note, other studies documented observed momentum flux, drag coefficient, and dissipative heating in the near-surface layer of landfalling TCs (e.g., Ming & Zhang, 2018; Zhang, Zhu, et al., 2011), despite no assessment of turbulent diffusion.

The present study aims to investigate the characteristics of turbulent momentum transfer over different types of underlying surfaces in the PBL of landfalling TCs with a focus on examining the behavior of the eddy viscosity. For the first time, the eddy viscosity will be examined for surface wind speeds >30 m s⁻¹ in the lower PBL (<100 m) of TCs under the contrast of ocean to land. The objective of this study is to compare the characteristics of turbulence parameters such as momentum flux, turbulent kinetic energy (TKE), dissipation rate, and eddy viscosity over land and coastal ocean to identify differences in the TCBL turbulence structure over surfaces with different roughness lengths.

2. Data and Analysis Method

High-frequency (10 Hz) wind data were collected by two towers during the landfalls of Typhoon Hagupit (2008) and Typhoon Chanthu (2010). Figures 1a and 1b show the storm tracks and tower locations. Details of the life cycles of the two typhoons are provided in Ming and Zhang (2018).

Tower 1 was located at 111.374°E, 21.439°N on the Zhizai Island which is separated from the mainland and is surrounded by shallow water (Figure 1c), so it is regarded as ocean in this study. The island has an above-water area of approximately 90 m × 40 m and is covered by sand and sparse weeds. On the other hand, Tower2 was installed close to farmland and residential areas (Figure 1d), which is regarded as land. The surface roughness length of two towers is calculated and documented by Ming and Zhang (2018, see their Figure 8), confirming that the surface roughness length at the location of Tower2 is much larger than that of Tower1. Fast response (10 Hz) sensors for 3D wind velocity and virtual temperature measurements were installed at 60 m height on Tower1 and at 70 m height on Tower2. The conventional observation systems for total wind speed measurements with a

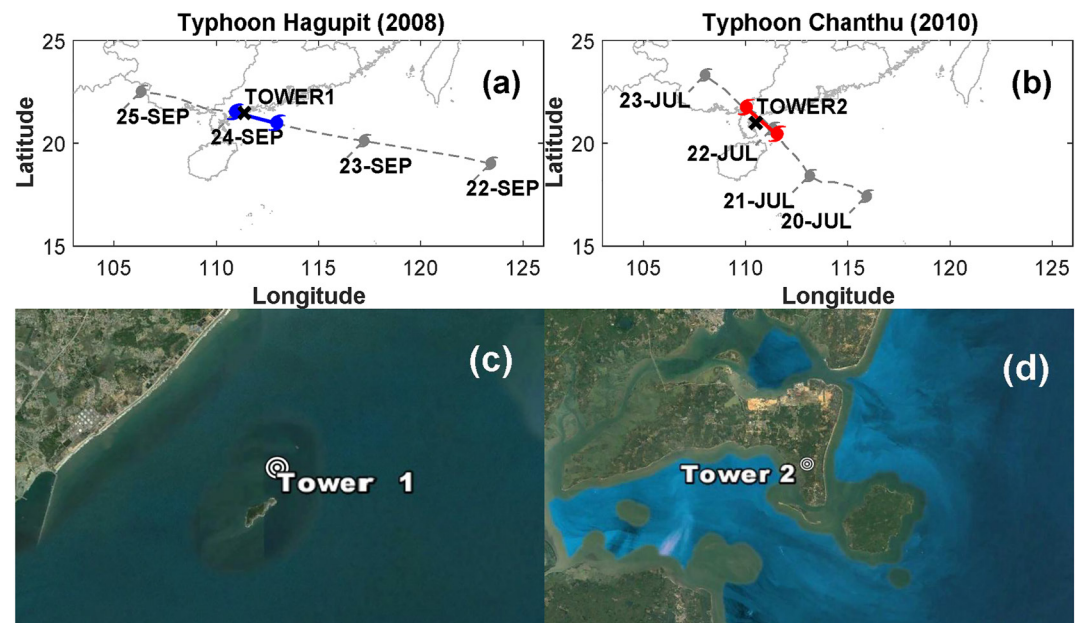


Figure 1. Plots of the locations of (a) Tower 1 with the track of Typhoon Hagupit (2008) and (b) Tower 2 with the track of Typhoon Chanthu (2010). Plots of the underlying surface conditions around (c) Tower 1 and (d) Tower 2. The blue and red colors represent the period we focused on during the two typhoons.

sample rate of 10 min were installed at 10, 20, 40, 60, 80, and 100 m on Tower1 and at 10, 30, 50, 70, and 100 m on Tower2. Note that the conventional systems failed at 60 and 80 m in Hagupit and at 50 and 70 m in Chanthu during the TC landfall periods.

The 10-min wind speeds during the periods of interest in the two typhoons are shown in Figure 2. The storm center of Typhoon Hagupit (2008) was close to Tower1 at 22 UTC on September 23 when the minimum wind speed of $\sim 10 \text{ m s}^{-1}$ was captured. The observed maximum wind speed at 100 m height by Tower1 reached $\sim 50 \text{ m s}^{-1}$ in Typhoon Hagupit when the eyewall passed by the tower (Figure 2a).

The wind speeds at three levels of Tower2 increased with time to a maximum of $\sim 35 \text{ m s}^{-1}$ at 100 m height when the eyewall of Typhoon Chanthu was closest to the tower and then generally decreased with time after the storm moved inland (Figure 2b). Both towers observed the general increasing trend of the wind speed with height at a given time. Due to the large roughness, the difference of wind speed at different levels is higher in the Typhoon Chanthu than that in the Typhoon Hagupit.

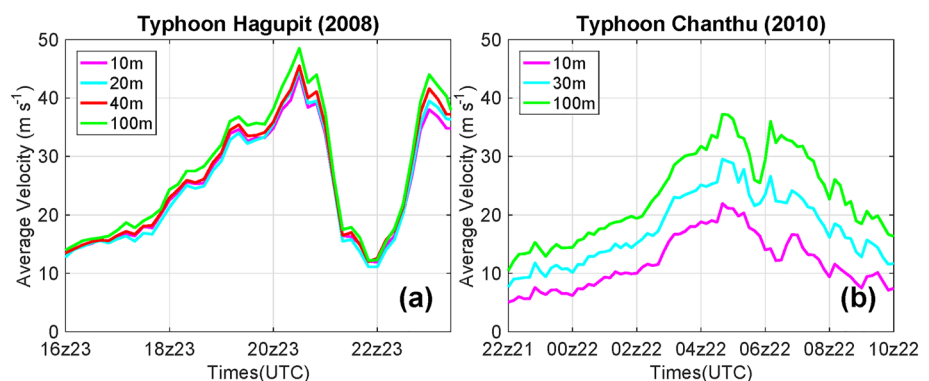


Figure 2. Timeseries of the 10-min wind speed at several levels in (a) Typhoon Hagupit (2008) from 16:00 UTC 23 September to 00:00 UTC 24 September 2008 (10 m, 20 m, 40 m, and 100 m, unit: m s^{-1}) measured by Tower1 and (b) Typhoon Chanthu (2010) from 22:00 UTC 21 July to 10:00 UTC 22 July 2010 measured by Tower2 (10 m, 30 m, and 100 m, unit: m s^{-1}).

The procedures of data processing and quality control followed those in Ming and Zhang (2018). The momentum flux is calculated using the standard eddy correlation method in the form of

$$\bar{\tau} = -\rho \left(\overline{u'w'i} + \overline{v'w'j} \right), \quad (1)$$

where ρ , u , v , and w represent the air density, along-wind, cross-wind, and vertical components of the three-dimensional wind velocities, respectively. The prime in Equation 1 represents the turbulent fluctuation of a variable, and the overbar represents time averaging over a 10 min period.

In a first-order closure PBL scheme, the momentum flux is usually calculated using the vertical eddy viscosity (K) and the strain rates as follows

$$|\bar{\tau}| = \rho K \left[\left(\frac{\partial u}{\partial z} \right)^2 + \left(\frac{\partial v}{\partial z} \right)^2 \right]^{1/2}, \quad (2)$$

where z is the height. The direct method for eddy viscosity estimation is to follow Equation 2 using both the flux and strain rates, which gives the following form

$$K = \frac{|\bar{\tau}|}{\rho} \left[\left(\frac{\partial u}{\partial z} \right)^2 + \left(\frac{\partial v}{\partial z} \right)^2 \right]^{-1/2}. \quad (3)$$

The turbulent kinetic energy (TKE, e) is calculated using the turbulent fluctuations as

$$e = \frac{1}{2} \left(\overline{u'^2} + \overline{v'^2} + \overline{w'^2} \right). \quad (4)$$

In the surface layer, the vertical eddy viscosity can be derived using the surface friction velocity (u_*) and height (z) following the Monin-Obukhov similarity theory (MOST), which has the following form

$$K1 = u_* \kappa z / \phi, \quad (5)$$

where $\kappa = 0.4$, ϕ is the stability function, and u_* is defined as

$$u_* = \left(\frac{|\bar{\tau}|}{\rho} \right)^{1/2}. \quad (6)$$

Following Donelan (1990), ϕ is a function of the Obukhov length (L) in the form of

$$\phi = \left(1 - 17 \frac{z}{L} \right)^{-1/4}; \text{ when } \frac{z}{L} < 0, \quad (7)$$

$$\phi = 1 + 5.4 \frac{z}{L}; \text{ when } \frac{z}{L} > 0. \quad (8)$$

L is defined as

$$L = \frac{-u_*^3 T_v}{\kappa g T_v' w'}, \quad (9)$$

where T_v stands for the virtual temperature, which is measured by the sonic anemometers. The method in Equation 5 is referred to as the theoretical method of determining $K1$ hereafter.

In a TKE-type PBL scheme (Holt & Raman, 1988), the effective vertical eddy viscosity (K_1) is usually parameterized using the TKE and dissipation rate (ϵ) in the form of

$$K2 = c_1 \frac{e^2}{\epsilon}, \quad (10)$$

where $c_1 = 0.03$ – 0.06 depending on the version of the TKE schemes (Beljaars et al., 1987; Detering & Etling, 1985). The method following Equation 10 for eddy viscosity calculation is referred to as the TKE method hereafter. The dissipation rate can be directly determined using the wind velocity spectrum in the form of

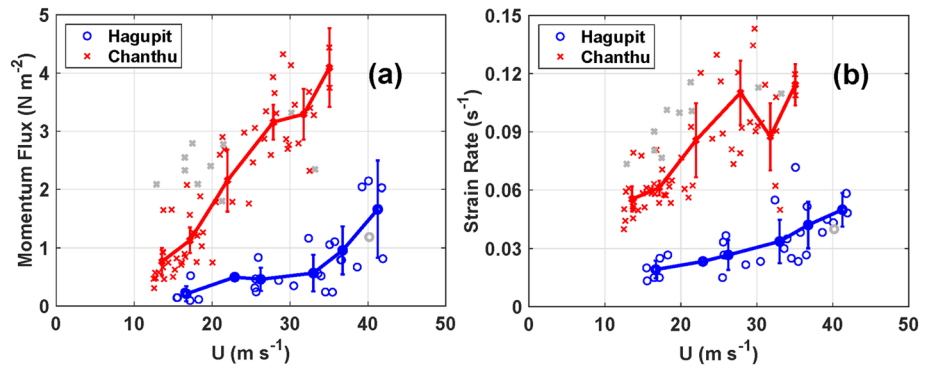


Figure 3. Plots of (a) momentum flux and (b) strain rate as a function of the mean wind speed at 60 m height in Typhoon Hagupit (2008, blue) and at 70 m height in Typhoon Chanthu (2010, red). The solid lines show the bin-averaged momentum flux and strain rate, and the error bars represent the 95% confidence interval. The gray markers stand for the data that are excluded from the eddy diffusivity calculations according to spectra analysis.

$$\varepsilon = \alpha_u^{-\frac{3}{2}} \frac{2\pi f}{U} [f S_{uu}(f)]^{\frac{3}{2}}, \quad (11)$$

where $\alpha_u = 0.5$ following Sreenivasan (1995), which is the non-dimensional Kolmogorov constant, U is the mean wind speed, f is the frequency and S is the power spectral density. Note that we removed few samples that slightly diverge from the Kolmogorov's $-5/3$ law so that our estimations for the dissipation rate hold. These deviations are perhaps due to the unsteady mesoscale forcing that makes the turbulent flow inhomogeneous and anisotropic.

Furthermore, we quantify the random error (R) in the flux calculation following Zhang and Montgomery (2012). This error is because a flux run is a finite sample of random processes. The random error is defined as:

$$R = \left(\frac{\sigma_F}{\bar{F}} \right) / \sqrt{N}, \quad (12)$$

where σ_F and \bar{F} are the standard deviation and mean of the fluxes and N is the total number of the flux runs. The random error is found to be 15.57% for Hagupit and 6.69% for Chanthu, which are much smaller than the aircraft observations of Zhang and Montgomery (2012).

3. Data Analysis Results

The momentum flux and strain rate are plotted as a function of the mean wind speed in Figures 3a and 3b, respectively, for both storms. Both the momentum flux and strain rate show an increasing trend with the mean wind speed. However, the magnitudes of these two parameters are much larger in Typhoon Chanthu than in Typhoon Hagupit at the same wind speed. Based on the bin (5 m s^{-1}) averaged value, the rate of increase of these two parameters with wind speed is larger in Typhoon Chanthu than in Typhoon Hagupit as indicated by the slope difference in the lines that connected the averaged values. This result indicates that the momentum transport and wind shear are larger over rougher surfaces in Typhoon Chanthu than over smoother surfaces in Typhoon Hagupit (c.f., Figure 1). Note that as mentioned in the method's section, we excluded a few samples (gray symbols in Figure 3), which did not follow $-5/3$ law in the inertial subrange of the energy spectrum, from our calculations. Radar reflectivity observations showed that such periods were associated with intense rainfall activity in the principal rainbands.

Figure 4 displays the relationship between the vertical eddy diffusivity estimated using the direct method (K) and wind speed for the two TCs. It is

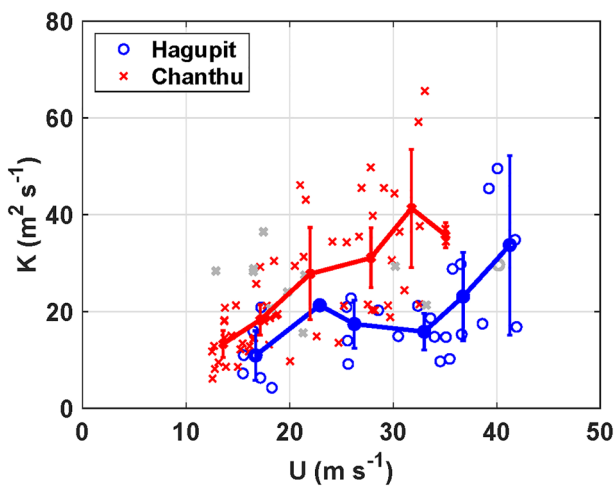


Figure 4. Plots of the vertical eddy diffusivity as a function of the mean wind speed using the direct method (K) at 60 m height in Typhoon Hagupit (2008, blue) and at 70 m height in Typhoon Chanthu (2010, red). The solid lines show the bin-averaged vertical eddy diffusivity estimated from the method, and the error bars represent the 95% confidence interval. The gray markers stand for the data that are excluded from the eddy diffusivity calculations according to spectra analysis.

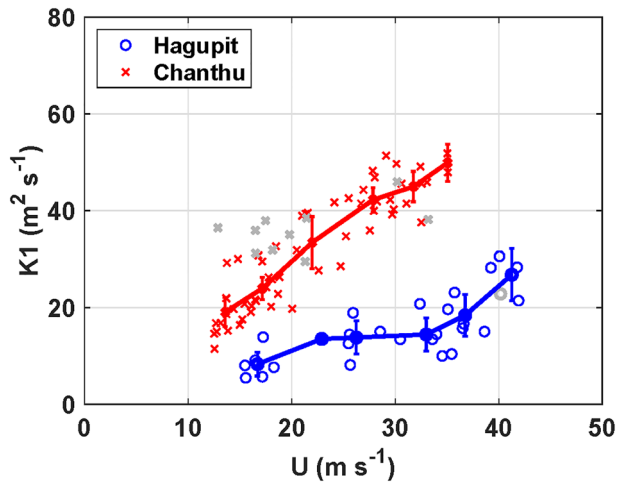


Figure 5. The same as Figure 4 but for the surface friction velocity method ($K1$).

evident that the eddy diffusivity generally increases with the mean wind speed in both storms. In Typhoon Chanthu, K levels off at wind speeds of $\sim 25 \text{ m s}^{-1}$ up to $\sim 35 \text{ m s}^{-1}$ and then increases at higher wind speeds. In Typhoon Hagupit, however, K continuously increases with the wind speed up to 33 m s^{-1} before leveling off. This level-off trend and different behaviors of K in these two cases need to be revisited when more observations are available.

At a given wind speed when there are observations in both storms, K is statistically significantly larger in Typhoon Chanthu than in Typhoon Hagupit. This result confirms that the strength of vertical turbulent mixing, as indicated by the eddy diffusivity, is larger over land where the surface roughness is larger than over the ocean (see Figure 8 of Ming & Zhang, 2018).

The vertical eddy diffusivity estimated using the theoretical method ($K1$) also shows a general increasing trend with the wind speed for both TCs (Figure 5). The level-off and re-increasing trend of $K1$ in Typhoon Hagupit is captured as that of K . It is evident that $K1$ is larger in Typhoon Chanthu than in Typhoon Hagupit at a given wind speed in a similar manner as the direct calculation of K . The difference in $K1$ between the two storms is larger than that in K at a

given wind speed. The reason for this different behavior of $K1$ will be discussed later. According to Equation 5, $K1$ is related to the surface friction velocity, height and stability function. Because the height is fixed and the stability function is close to 1, $K1$ mainly depends on the surface friction velocity (u_*). Using the log-law, we can estimate the ratio of $u_{*,land}/u_{*,ocean} = \ln(z/z_{0,ocean})/\ln(z/z_{0,land}) \sim 2$ assuming typical values of $z_{0,ocean} = 10^{-4} \text{ m}$ and $z_{0,land} = 0.1 \text{ m}$, which are the mean values of the surface roughness length from Tower1 and Tower2, respectively following Ming and Zhang (2018). As can be seen from Figure 5, $K1_{land}/K1_{ocean}$ has approximately a similar ratio. Since the surface friction velocity is the square root of the momentum flux, it is expected to see a similar behavior of $K1$ as K .

The TKE and dissipation rate as a function of the mean wind speed are shown in Figure 6. As expected, the TKE generally increases with the wind speed in both TCs in a similar manner as the momentum flux. The TKE is much larger in Typhoon Chanthu than in Typhoon Hagupit at the same wind speed (Figure 6a), indicating that the turbulence intensity is larger over land than over ocean under the same surface wind regime.

The dissipation rate also increases with the wind speed in both cases (Figure 6b), which is the same as the result of Ming and Zhang (2018). The rate of increase of the dissipation rate with wind speed is much larger under high wind conditions ($>25 \text{ m s}^{-1}$) than at lower wind speeds. The dissipation rate is larger in Typhoon Chanthu than in Typhoon Hagupit at the same wind speed (Figure 6b), suggesting that the rougher land surfaces cause larger dissipation due to larger surface friction than ocean surfaces.

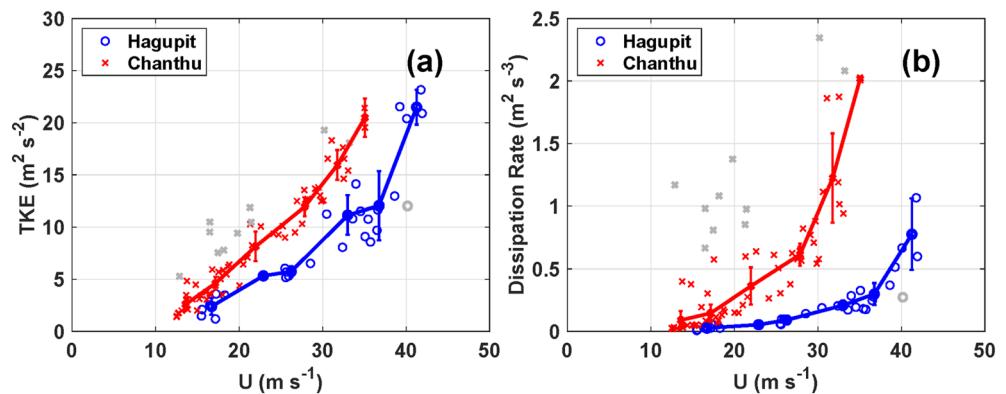


Figure 6. Plots of (a) TKE and (b) dissipation rate as a function of the mean wind speed in at 60 m height Typhoon Hagupit (2008, blue) and at 70 m height in Typhoon Chanthu (2010, red). The solid lines show the bin-averaged momentum flux and strain rate, and the error bars represent the 95% confidence interval. The gray markers stand for the data that are excluded from the eddy diffusivity calculations according to spectra analysis.

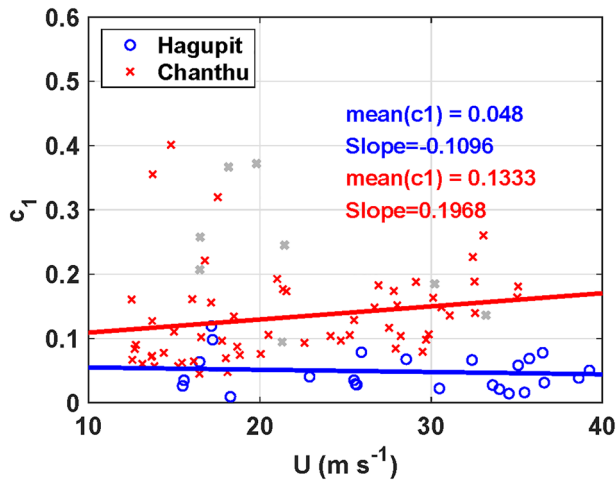


Figure 7. Plots of the constant c_1 in the TKE method as a function of the mean wind speed in Typhoon Hagupit (2008, blue) and Typhoon Chanthu (2010, red). The red and blue solid lines represent the least-square-best fit in Chanthu and Hagupit, respectively. The gray markers stand for the data that are excluded from the eddy diffusivity calculations according to spectra analysis.

Using the TKE method, K_2 is very small in Typhoon Chanthu when the scaling coefficient $c_1 = 0.03\text{--}0.006$ from the TKE schemes compared to K from the direct method (not shown). Thus, the vertical eddy diffusivity estimated by the direct method is treated as the true value, and the c_1 is calculated with the TKE and dissipation rate in both TCs. Note that the mean value of c_1 in two storms with all data used in the calculation is treated as the scaling coefficient in the TKE method (i.e., for K_2 calculation).

Figure 7 shows the relationship between c_1 and wind speed in the two storms. The small correlation coefficients indicate that c_1 and wind speed are generally independent of each other and thus c_1 is not a function of wind speed. The mean value of c_1 in Typhoon Chanthu (0.133) is much larger than that in Typhoon Hagupit (0.048). This result suggests that the constant c_1 used in the TKE method (Equation 10) may be different over land versus over ocean. Figure 7 indicates that c_1 in Equation 10 is not a universal coefficient and c_1 in the TKE method should be treated as a different value when the underlying surface is different. Over the ocean, c_1 should be 0.02–0.12. However, c_1 should be 0.05–0.4 when the underlying surface is land based on the backward calculation of this coefficient using K from the direct flux method. The difference in c_1 between land and ocean is due to different influences of surface roughness types on TKE and dissipation rate. As a result, c_1 increases with the surface roughness.

The vertical eddy diffusivity estimated using the TKE method (K_2) using the mean values of the observed c_1 for each storm based on Figure 7 is shown in

Figure 8 as a function of wind speed. K_2 also generally increases with the mean wind speed in both TCs. The variation pattern of K_2 with wind speed is very similar to that of K and K_1 in both storms. The degree of enhancement of the dissipation rate by increasing the surface roughness is larger than that of the TKE relative to the values over a smooth surface, so that the ratio of TKE and dissipation rate that governs the magnitude of K_2 becomes much smaller when the surface roughness is large.

The scatter distribution comparing the vertical eddy diffusivity between the direct and theoretical methods from the two typhoons is shown in Figure 9. The total least-square-best fit gave the regression relationship between K and K_1 . $K_1 = 0.6902 K + 9.0794$ with a correlation coefficient of 0.87 for Typhoon Hagupit, and $K_1 = 0.5692 K + 12.5078$ with a correlation coefficient of 0.85 for Typhoon Chanthu. Furthermore, the regression relationship between K and K_1 using all data of both storms is $K_1 = 0.9823 K + 3.3942$ with a correlation coefficient of 0.92. Since the theoretical method is based on surface layer similarity theory, the measurement height is assumed to be within surface layer depth. The Monin-Obukhov similarity theory holds in both cases according to observed logarithmic wind profiles (Ming & Zhang, 2018).

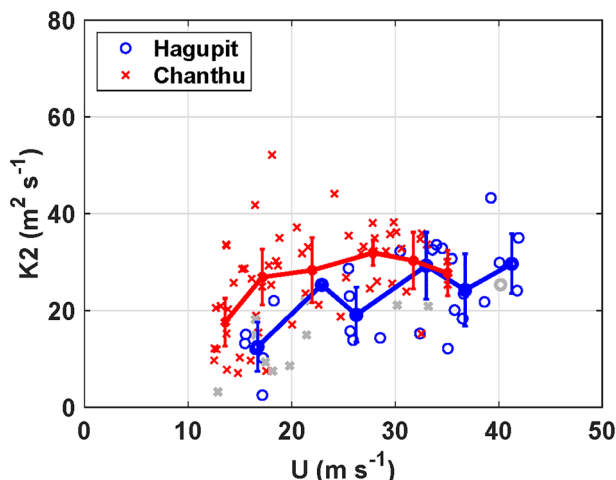


Figure 8. The same as Figure 4, but for TKE method (K_2) using the mean c_1 for each storm from Figure 7.

The scatter plot in Figure 10 compares the vertical eddy diffusivity estimated using the direct and TKE methods. Interestingly, K_2 is mostly larger than K in both TCs. The regression equations based on the total least square best fit are $K_2 = 0.5853 K + 4.1505$ for Typhoon Hagupit, and $K_2 = 0.8422 K + 10.8522$ for Typhoon Chanthu, respectively. The regression relationship between K and K_2 using all data of the two storms is $K_2 = 0.6023 K + 11.3942$. Furthermore, the correlation coefficient is 0.354 for Typhoon Hagupit, and 0.521 for Typhoon Chanthu, respectively. Note that the correlation coefficient is improved from ~ 0.06 to ~ 0.5 using the corrected c_1 for both storms. However, the correlation coefficient between K_2 and K is still smaller than that of K_1 versus K . This result suggests that the TKE method produces larger variance in the eddy diffusivity estimates than the theoretical method in the TC surface layer.

4. Discussion and Conclusions

Based on the high-frequency wind data collected by multiple-level towers, turbulent parameters such as momentum flux, strain rate, TKE, dissipation

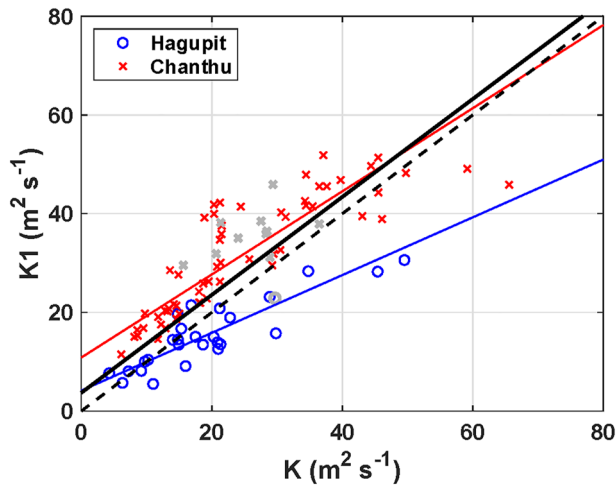


Figure 9. Comparisons of vertical eddy diffusivity estimated by the direct method and the surface friction velocity method in (a) Typhoon Hagupit (2008, blue) and (b) Typhoon Chanthu (2010, red). The gray markers stand for the data that are excluded from the eddy diffusivity calculations according to spectra analysis. The blue and red solid lines represent the total least-square-best fits for Hagupit and Chanthu, respectively. The black dashed lines represent a ratio of 1:1, and the black solid lines represent the total least-square-best fit using all data (blue, red, and gray).

of Hurricane Dennis (2015) are also shown in S1. Enhancement of the vertical eddy diffusivity overland in HWRF led to improvements in the track and intensity of Hurricane Dennis (Figure S1 in Supporting Information S1). Increasing the vertical eddy diffusivity induces smaller boundary layer inflow, smaller convergence, smaller adiabatic force, and less radial advection of absolute angular momentum at the eyewall region, which in turn weakens the storm more rapidly than in the unmodified case (Figures S2 and S3 in Supporting Information S1). This chain of the physical processes and TC intensity change due to the change of vertical eddy diffusivity is consistent with previous studies (e.g., Zhang et al., 2015).

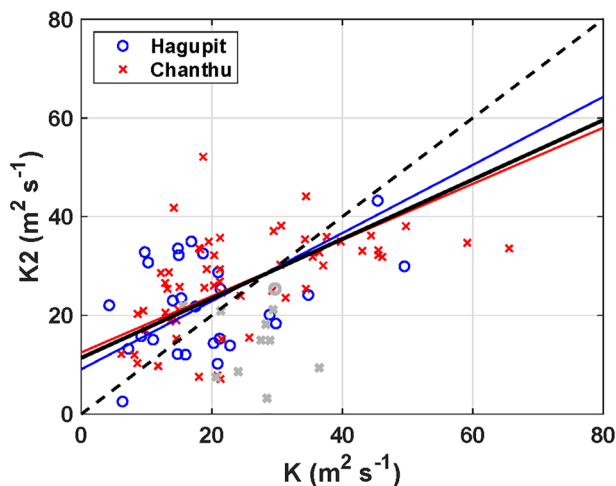


Figure 10. Comparisons of vertical eddy diffusivity estimated by the direct method and the TKE method in (a) Typhoon Hagupit (2008, blue) and (b) Typhoon Chanthu (2010, red). The gray markers stand for the data that are excluded from the eddy diffusivity calculations according to spectra analysis. The blue and red solid lines represent the total least-square-best fits for Hagupit and Chanthu, respectively. The black dashed lines represent a ratio of 1:1, and the black solid lines represent the total least-square-best fit using all data (blue, red, and gray).

rate and vertical eddy diffusivity are examined during two TC landfalls. The results show that all these considered parameters have a general increasing trend with the wind speed. The magnitudes of these turbulent properties based on direct turbulence and wind observations are much larger over land than over the coastal ocean for a given wind speed.

As mentioned earlier, vertical eddy diffusivity plays a vital role in hurricane forecasts and simulations (e.g., Gopalakrishnan et al., 2013; Zhang et al., 2015; F. Zhang et al., 2017; J. A. Zhang et al., 2017; Zhang & Pu, 2017). Our result suggests that the vertical eddy diffusivity has different characteristics over different roughness under the same surface wind speeds. All three methods show that the vertical eddy diffusivity is larger over land than over ocean. This result is consistent with observations of eddy diffusivity over land comparing estimates from onshore versus offshore (Tang et al., 2018), as well as numerical simulations of landfalling TCs (Zhang & Pu, 2017; F. Zhang et al., 2017; Momen et al., 2021).

The difference in vertical eddy diffusivity with different underlying surfaces in the boundary layer scheme should be considered in TC models. To show the significance of the surface roughness impacts on hurricane dynamics, we modified the vertical mixing strength within the NCEP HWRF system. We carried out a control run with the default HWRF and another simulation by multiplying a factor of 1.89 based on the tower observations to the vertical eddy diffusivity in the PBL scheme over land. Details of the model setup are shown in Supporting Information S1 (Text S1). Results of a sensitivity experiment that test the effects of the modified eddy diffusivity on the structure and intensity of Hurricane Dennis (2015) are also shown in S1. Enhancement of the vertical eddy diffusivity overland in HWRF led to improvements in the track and intensity of Hurricane Dennis (Figure S1 in Supporting Information S1). Increasing the vertical eddy diffusivity induces smaller boundary layer inflow, smaller convergence, smaller adiabatic force, and less radial advection of absolute angular momentum at the eyewall region, which in turn weakens the storm more rapidly than in the unmodified case (Figures S2 and S3 in Supporting Information S1). This chain of the physical processes and TC intensity change due to the change of vertical eddy diffusivity is consistent with previous studies (e.g., Zhang et al., 2015).

All three methods show that the vertical eddy diffusivity increases with the wind speed, which agrees with previous studies (e.g., Tang et al., 2018; Zhang & Drennan, 2012; Zhang, Marks, et al., 2011). The degree of change of the vertical eddy diffusivity with the wind speed is different when the underlying surface roughness is different. When the roughness is larger, the vertical eddy diffusivity more quickly increases with the wind speed. Hence, the roughness length is suggested to be considered as an additional variable in any vertical eddy diffusivity parameterization.

The vertical eddy diffusivity directly estimated using the momentum flux and strain rate is compared to that estimated using the friction velocity and height based on the Monin-Obukhov similarity theory (MOST). Our result shows that the eddy diffusivity based on the direct method is comparable to that based on MOST over both ocean and land. Our results agree with Tang et al. (2018). Note that Dropsonde and Doppler radar observations in Hurricane Irene (2011) showed that the boundary layer jet is deeper over land (Alford et al., 2020) than over ocean, implying that the surface layer is deeper over land. Since we only have one layer flux data, this hypothesis could not be verified using our data. Future work is recommended to collect multilevel flux observations to explore the evolution of surface layer depth from ocean to land in TCs.

Our results also show the different scaling coefficients should be used in the TKE method for parameterizing the vertical eddy diffusivity over ocean and

land. In fact, we showed that the surface roughness affects the vertical eddy diffusion estimation based on TKE. The TKE method with observation-based scaling coefficients improved the correlation with the direct method. More observations are needed to further understand how other types of surfaces than those in this study affect turbulent mixing during TC landfalls. The underlying mechanisms for turbulence generation and dissipation may be explored using high-resolution large eddy simulations that resolve turbulent eddies (e.g., Li et al., 2021; Momen et al., 2021). The uniqueness of the data set used in this study is that the observation heights are sufficiently low so that the eddy diffusivities are reasonably well predicted by MOST. Our results suggested that the tower data are either in the MOST layer or in the matching layer between the inner (MOST layer) and outer (main portion) PBL solutions. Scaling the TKE closures for the MOST/matching layer to converge into the MOST scaling will potentially improve the TKE schemes. Future work will focus on finding a condition on the scaling parameter (c_1) in the TKE closure, and hence an improved model for it, that extends into the outer PBL using field observations.

Data Availability Statement

The observed data used in this paper are available on <https://box.nju.edu.cn/d/dcbefdd2bcd24446b350/> with a password of datajgr for downloading the data. The hurricane field experiment data can be accessed through https://www.aoml.noaa.gov/hrd/data_sub/hurr.html. Access to other public datasets used in this study is described in Ming and Zhang (2018) that can be obtained from <https://doi.org/10.1029/2017JD028076>.

References

- Alford, A. A., Zhang, J. A., Biggerstaff, M. I., Dodge, P., & Bodine, D. J. (2020). Transition of the hurricane boundary layer during the landfall of hurricane Irene (2011). *Journal of the Atmospheric Sciences*, 77(10), 3509–3531. <https://doi.org/10.1175/jas-d-19-0290.1>
- Beljaars, A. C. M., Walmsley, J. L., & Talor, P. A. (1987). A mixed spectral finite-difference model for neutrally stratified boundary layer flow over roughness changes and topography. *Boundary-Layer Meteorology*, 38(3), 273–303. <https://doi.org/10.1007/bf00122448>
- Braun, S. A., & Tao, W.-K. (2000). Sensitivity of high-resolution simulations of hurricane Bob (1991) to planetary boundary layer parameterizations. *Monthly Weather Review*, 128(12), 3941–3961. [https://doi.org/10.1175/1520-0493\(2000\)129<3941:sohrso>2.0.co;2](https://doi.org/10.1175/1520-0493(2000)129<3941:sohrso>2.0.co;2)
- Bryan, G. H. (2012). Effects of surface exchange coefficients and turbulence length scales on the intensity and structure of numerically simulated hurricanes. *Monthly Weather Review*, 140(4), 1125–1143. <https://doi.org/10.1175/mwr-d-11-00231.1>
- Bryan, G. H., & Rotunno, R. (2009). Evaluation of an analytical model for the maximum intensity of tropical cyclones. *Journal of the Atmospheric Sciences*, 66(10), 3042–3060. <https://doi.org/10.1175/2009jas3038.1>
- Bu, Y. P., Fovell, R. G., & Corbosiero, K. L. (2017). The influence of boundary layer mixing and cloud-radiative forcing on tropical cyclone size. *Journal of the Atmospheric Sciences*, 74(4), 1273–1292. <https://doi.org/10.1175/jas-d-16-0231.1>
- Chen, X., Bryan, G. H., Zhang, J. A., Cione, J. J., & Marks, F. D. (2021). A framework for simulating the tropical-cyclone boundary layer using large-eddy simulation and its use in evaluating PBL parameterizations. *Journal of the Atmospheric Sciences*, 78(11), 3559–3574. <https://doi.org/10.1175/jas-d-20-0227.1>
- Cione, J. J., Bryan, G. H., Dobosy, R., Zhang, J. A., de Boer, G., Aksoy, A., et al. (2020). Eye of the storm: Observing hurricanes with a small unmanned aircraft system. *Bulletin of the American Meteorological Society*, 101(2), E186–E205. <https://doi.org/10.1175/bams-d-19-0169.1>
- Detering, H. W., & Etling, D. (1985). Application of the E-E turbulence model to the atmospheric boundary layer. *Boundary-Layer Meteorology*, 33(2), 113–133. <https://doi.org/10.1007/bf00123386>
- Donelan, M. A. (1990). Air–sea interaction. *The Sea: Ocean Engineering Science*, 9, 279–280.
- Emanuel, K. A. (1995). Sensitivity of tropical cyclones to surface exchange coefficients and a revised steady-state model incorporating eye dynamics. *Journal of the Atmospheric Sciences*, 52(22), 3969–3976. [https://doi.org/10.1175/1520-0469\(1995\)052<3969:soctcs>2.0.co;2](https://doi.org/10.1175/1520-0469(1995)052<3969:soctcs>2.0.co;2)
- Emanuel, K. A. (1997). Some aspects of hurricane inner-core dynamics and energetics. *Journal of the Atmospheric Sciences*, 54(8), 1014–1026. [https://doi.org/10.1175/1520-0469\(1997\)054<1014:saohic>2.0.co;2](https://doi.org/10.1175/1520-0469(1997)054<1014:saohic>2.0.co;2)
- Emanuel, K. A. (2012). Self-stratification of tropical cyclone outflow. Part II: Implications for storm intensification. *Journal of the Atmospheric Sciences*, 69(3), 988–996. <https://doi.org/10.1175/jas-d-11-0177.1>
- Foster, R. C. (2009). Boundary-layer similarity under an axisymmetric, gradient wind vortex. *Boundary-Layer Meteorology*, 131(3), 321–344. <https://doi.org/10.1007/s10546-009-9379-1>
- Gopalakrishnan, S. G., Marks, F. D., Jr., Zhang, J. A., Zhang, X., Bao, J.-W., & Tallapragada, V. (2013). A study of the impacts of vertical diffusion on the structure and intensity of the tropical cyclones using the high-resolution HWRF system. *Journal of the Atmospheric Sciences*, 70(2), 524–541. <https://doi.org/10.1175/jas-d-11-0340.1>
- Holt, T., & Raman, S. (1988). A review and comparative evaluation of multilevel boundary layer parameterization for first-order and turbulent kinetic energy closure schemes. *Reviews of Geophysics*, 26(4), 761–780. <https://doi.org/10.1029/rg026i004p00761>
- Keper, J. D. (2012). Choosing a boundary layer parameterization for tropical cyclone modeling. *Monthly Weather Review*, 140(5), 1427–1445. <https://doi.org/10.1175/mwr-d-11-00217.1>
- Li, M., Zhang, J. A., Matak, L., & Momen, M. (2023). The impacts of adjusting momentum roughness length on strong and weak hurricane forecasts: A comprehensive analysis of weather simulations and observations. *Monthly Weather Review*, 151(5), 1287–1302. <https://doi.org/10.1175/MWR-D-22-0191.1>
- Li, X., Pu, Z., & Gao, Z. (2021). Effects of roll vortices on the evolution of hurricane harvey during landfall. *Journal of the Atmospheric Sciences*, 78(6), 1847–1867.
- Ma, Z., Fei, J., Huang, X., & Cheng, X. (2018). Sensitivity of the simulated tropical cyclone intensification to the boundary-layer height based on a K-profile boundary-layer parameterization scheme. *Journal of Advances in Modeling Earth Systems*, 10(11), 2912–2932. <https://doi.org/10.1029/2018ms001459>

Acknowledgments

Jie Ming acknowledges support from the National Natural Science Foundation of China (Grant 42192555) and Fundamental Research Funds for the Central Universities (No. 020714380171). Jun Zhang acknowledges supports from the National Oceanic and Atmospheric Administration (NOAA) Grants NA21OAR4590370, NA22OAR4590178, and NA22OAR4050669D, and NA19OAR4590239, National Science Foundation (NSF) Awards 2228299 and 2211308, and the U.S. Office of Naval Research Grant N00014-20-1-2071. Zhaoxia Pu and Xin Li acknowledge supports from the NOAA Grant NA19OAR4590239 and National Science Foundation Award OAC2004658. Mostafa Momen acknowledges support from the Department of Civil and Environmental Engineering at the University of Houston. We are grateful to Frank Marks for his helpful comments and suggestions that have helped improve the paper. The scientific results and conclusions, as well as any views or opinions expressed herein, are those of the authors and do not necessarily reflect those of OAR or the Department of Commerce.

- Ming, J., & Zhang, J. A. (2018). Direct measurements of momentum flux and dissipative heating in the surface layer of tropical cyclones during landfalls [Dataset]. *Journal of Geophysical Research: Atmospheres*, *123*(10), 4926–4938. <https://doi.org/10.1029/2017JD028076>
- Momen, M., Parlange, M. B., & Giometto, M. G. (2021). Scrambling and reorientation of classical atmospheric boundary layer turbulence in hurricane winds. *Geophysical Research Letters*, *48*(7), e2020GL091695. <https://doi.org/10.1029/2020gl091695>
- Montgomery, M. T., & Smith, R. K. (2014). Paradigms for tropical-cyclone intensification. *Australian Meteorological and Oceanographic Journal*, *64*(1), 37–66. <https://doi.org/10.22499/2.6401.005>
- Nolan, D. S., Stern, D. P., & Zhang, J. A. (2009). Evaluation of planetary boundary layer parameterizations in tropical cyclones by comparison of in situ data and high-resolution simulations of Hurricane Isabel (2003). Part II: Inner core boundary layer and eyewall structure. *Monthly Weather Review*, *137*(11), 3675–3698. <https://doi.org/10.1175/2009mwr2786.1>
- Romdhani, O., Zhang, J. A., & Momen, M. (2022). The impact of turbulence closures on real hurricane forecasts: A comprehensive joint assessment of grid resolution, turbulence models, and horizontal diffusion parameters. *Journal of Advances in Modeling Earth Systems*, *14*, e2021MS002796. <https://doi.org/10.1029/2021MS002796>
- Rotunno, R., & Bryan, G. H. (2012). Effects of parameterized diffusion on simulated hurricanes. *Journal of the Atmospheric Sciences*, *69*(7), 2284–2299. <https://doi.org/10.1175/jas-d-11-0204.1>
- Smith, R. K., & Thomsen, G. L. (2010). Dependence of tropical-cyclone intensification on the boundary layer representation in a numerical model. *Quarterly Journal of the Royal Meteorological Society*, *136*(652), 1671–1685. <https://doi.org/10.1002/qj.687>
- Sreenivasan, K. R. (1995). On the universality of the Kolmogorov constant. *Physics of Fluids*, *7*(11), 2778–2784. <https://doi.org/10.1063/1.868656>
- Tang, J., Zhang, J. A., Aberson, S. D., Marks, F. D., & Lei, X. (2018). Multilevel tower observations of vertical eddy diffusivity and mixing length in the tropical cyclone boundary layer during landfalls. *Journal of the Atmospheric Sciences*, *75*(9), 3159–3168. <https://doi.org/10.1175/jas-d-17-0353.1>
- Wang, W., Sippel, J. A., Abarca, S., Zhu, L., Liu, B., Zhang, Z., et al. (2018). Improving NCEP HWRF simulations of surface wind and inflow angle in the eyewall area. *Weather and Forecasting*, *33*(3), 887–898. <https://doi.org/10.1175/waf-d-17-0115.1>
- Zhang, F., & Pu, Z. (2017). Effects of vertical eddy diffusivity parameterization on the evolution of landfalling hurricanes. *Journal of the Atmospheric Sciences*, *74*(6), 1879–1905. <https://doi.org/10.1175/jas-d-16-0214.1>
- Zhang, F., Pu, Z., & Wang, C. (2017a). Effects of boundary layer vertical mixing strength on the evolution of hurricanes over land. *Monthly Weather Review*, *145*(6), 2343–2361. <https://doi.org/10.1175/mwr-d-16-0421.1>
- Zhang, J. A., Drennan, W. M., Black, P. G., & French, J. R. (2009). Turbulence structure of the hurricane boundary layer between the outer rainbands. *Journal of the Atmospheric Sciences*, *66*(8), 2455–2467. <https://doi.org/10.1175/2009jas2954.1>
- Zhang, J. A., & Drennan, W. M. (2012). An observational study of vertical eddy diffusivity in the hurricane boundary layer. *Journal of the Atmospheric Sciences*, *69*(11), 3223–3236. <https://doi.org/10.1175/jas-d-11-0348.1>
- Zhang, J. A., Kalina, E. A., Biswas, M. K., Rogers, R. F., Zhu, P., & Marks, F. D. (2020). A review and evaluation of planetary boundary layer parameterizations in Hurricane Weather Research and Forecasting model using idealized simulations and observations. *Atmosphere*, *11*(10), 1091. <https://doi.org/10.3390/atmos11101091>
- Zhang, J. A., & Marks, F. D. (2015). Effects of horizontal diffusion on tropical cyclone intensity change and structure in idealized three-dimensional numerical simulations. *Monthly Weather Review*, *143*(10), 3981–3995. <https://doi.org/10.1175/mwr-d-14-00341.1>
- Zhang, J. A., Marks, F. D., Montgomery, M. T., & Loruso, S. (2011). An estimation of turbulent characteristics in the low-level region of intense Hurricanes Allen (1980) and Hugo (1989). *Monthly Weather Review*, *139*(5), 1447–1462. <https://doi.org/10.1175/2010mwr3435.1>
- Zhang, J. A., Marks, F. D., Sippel, J. A., Rogers, R. F., Zhang, X., Gopalakrishnan, S. G., et al. (2018). Evaluating the impact of improvement in the horizontal diffusion parameterization on hurricane prediction in the operational Hurricane Weather Research and Forecasting (HWRF) model. *Weather and Forecasting*, *33*(1), 317–329. <https://doi.org/10.1175/WAF-D-17-0097.1>
- Zhang, J. A., & Montgomery, M. T. (2012). Observational estimates of the horizontal eddy diffusivity and mixing length in the low-level region of intense hurricanes. *Journal of the Atmospheric Sciences*, *69*(4), 1306–1316. <https://doi.org/10.1175/jas-d-11-0180.1>
- Zhang, J. A., Nolan, D. S., Rogers, R. F., & Tallapragada, V. (2015). Evaluating the impact of improvements in the boundary layer parameterizations on hurricane intensity and structure forecasts in HWRF. *Monthly Weather Review*, *143*(8), 3136–3154. <https://doi.org/10.1175/mwr-d-14-00339.1>
- Zhang, J. A., & Rogers, R. F. (2019). Effects of parameterized boundary layer structure on hurricane rapid intensification in shear. *Monthly Weather Review*, *147*(3), 853–871. <https://doi.org/10.1175/mwr-d-18-0010.1>
- Zhang, J. A., Rogers, R. F., & Tallapragada, V. (2017b). Impact of parameterized boundary layer structure on tropical cyclone rapid intensification forecasts in HWRF. *Monthly Weather Review*, *145*(4), 1413–1426. <https://doi.org/10.1175/mwr-d-16-0129.1>
- Zhang, J. A., Zhu, P., Masters, F. J., Rogers, R. F., & Marks, F. D. (2011). On momentum transport and dissipative heating during hurricane landfalls. *Journal of the Atmospheric Sciences*, *68*(6), 1397–1404. <https://doi.org/10.1175/jas-d-10-05018.1>
- Zhao, Z., Chan, P. W., Wu, N., Zhang, J. A., & Hon, H. H. (2020). Aircraft observations of turbulence characteristics in the tropical cyclone boundary layer. *Boundary-Layer Meteorology*, *174*(3), 493–511. <https://doi.org/10.1007/s10546-019-00487-8>
- Zhu, P., Menelaou, K., & Zhu, Z.-D. (2014). Impact of subgrid-scale vertical turbulent mixing on eyewall asymmetric structures and mesovortices of hurricanes. *Quarterly Journal of the Royal Meteorological Society*, *140*(679), 416–438. <https://doi.org/10.1002/qj.2147>

References From the Supporting Information

- Biswas, M. K., Carson, L., Holt, C., & Bernardet, L. (2015). Community HWRF users's Guidev3.7a (p. 150).
- Ferrier, B. S., Jin, Y., Lin, Y., Black, T., & Dimego, G. (2002). Implementation of a new grid-scale cloud and precipitation scheme in the NCEP Eta model. In *Preprints, 15th conf. On numerical weather prediction*. In *Amer. Meteor. Soc.* (pp. 280–283).
- Hong, S. Y., & Pan, H. L. (1996). Nonlocal boundary layer vertical diffusion in a medium-range forecast model. *Monthly Weather Review*, *124*(10), 2322–2339. [https://doi.org/10.1175/1520-0493\(1996\)124<2322:nblvdi>2.0.co;2](https://doi.org/10.1175/1520-0493(1996)124<2322:nblvdi>2.0.co;2)
- Hong, S. Y., & Pan, H. L. (1998). Convective trigger function for a mass-flux cumulus parameterization scheme. *Monthly Weather Review*, *126*(10), 2599–2620. [https://doi.org/10.1175/1520-0493\(1998\)126<2599:ctffam>2.0.co;2](https://doi.org/10.1175/1520-0493(1998)126<2599:ctffam>2.0.co;2)
- Janjić, Z. I., Gall, R., & Pyle, M. E. (2010). Scientific documentation for the NMM solver. NCAR Tech (pp.53). Note NCAR/TN–477+STR. <https://doi.org/10.5065/D6MW2F3Z>
- Kurihara, Y., & Tuleya, R. E. (1974). Structure of a tropical cyclone developed in a three-dimensional numerical simulation model. *Journal of the Atmospheric Sciences*, *31*(4), 893–919. [https://doi.org/10.1175/1520-0469\(1974\)031<0893:soatcd>2.0.co;2](https://doi.org/10.1175/1520-0469(1974)031<0893:soatcd>2.0.co;2)
- Lacis, A. A., & Hansen, J. E. (1974). A parameterization for the absorption of solar radiation in the earth's atmosphere. *Journal of the Atmospheric Sciences*, *31*(1), 118–133. [https://doi.org/10.1175/1520-0469\(1974\)031<0118:apftao>2.0.co;2](https://doi.org/10.1175/1520-0469(1974)031<0118:apftao>2.0.co;2)

- Pan, H. L., & Wu, J. (1995). Implementing a mass flux convection parameterization package for the NMC medium-range forecast model. NMC Office Note 409 (pp. 40).
- Schwarzkopf, M. D., & Fels, S. (1991). The simplified exchange method revisited: An accurate, rapid method for computation of infrared cooling rates and fluxes. *Journal of Geophysical Research*, 96(D5), 9075–9096. <https://doi.org/10.1029/89jd01598>
- Sirutis, J. J., & Miyakoda, K. (1990). Subgrid scale physics in 1-month forecasts. Part I: Experiment with four parameterization packages. *Monthly Weather Review*, 118(5), 1043–1064. [https://doi.org/10.1175/1520-0493\(1990\)118<1043:sspimf>2.0.co;2](https://doi.org/10.1175/1520-0493(1990)118<1043:sspimf>2.0.co;2)
- Troen, I. B., & Mahrt, L. (1986). A simple model of the atmospheric boundary layer; sensitivity to surface evaporation. *Boundary-Layer Meteorology*, 37(1–2), 129–148. <https://doi.org/10.1007/bf00122760>
- Tuleya, R. E. (1994). Tropical storm development and decay: Sensitivity to surface boundary conditions. *Monthly Weather Review*, 122(2), 291–304. [https://doi.org/10.1175/1520-0493\(1994\)122<0291:tsdads>2.0.co;2](https://doi.org/10.1175/1520-0493(1994)122<0291:tsdads>2.0.co;2)